One Dimensional Simulations of Cerebral Blood Flow

Elizabeth Cheever

Applied Mathematics

Brown University

A thesis submitted for Honors for the degree of

Sc.B. Applied Mathematics - Computer Science

May 2009

Dedication

To my wonderful parents, Mary and Dick, who provide me with unconditional love and support. Thank you for your guidance over the past 21 years. Thank you, Mom, for inspiring me to pursue my dreams. Thank you, Dad, for sparking my interest in the world of mathematics. I love you!

To my grandfather, James Meehan, who has always been my biggest fan, given me invaluable advice, and impressed upon me the importance of education. I love you very much.

"Learn all you can, Elizabeth, and you'll never be sorry."
This thesis is for you, Grandpa.

Acknowledgements

First I would like to thank my thesis advisor, Professor George Karniadakis of the Brown University Applied Mathematics Department. Thank you for your guidance and support.

To Professor Peter Richardson of the Division of Engineering and Department of Molecular Pharmacology, Physiology, and Biotechnology of Brown University, I extend a big thank you. I appreciate your insight and the time you spent teaching me about fluid dynamics.

This thesis would not have been possible without the support and direction I received from Leopold Grinberg, an Applied Mathematics PhD candidate at Brown University. Thank you for spending many hours teaching me about cerebral blood flow and about the one-dimensional model.

Contents

List of Figures

List of Tables

1

Introduction

The health of the human brain is dependent on cerebral blood flow, which is the means of carrying oxygen and nutrients to the brain. These nutrients are brought to the brain via a complex network of arteries which are tightly regulated by many temporal and spatial constraints. The regulation is based on the viscosity of the blood, the pressure of blood flow into the brain, the cross-sectional area of the arteries, and other factors. The diameters of arteries are constantly changing via the process or autoregualtion. The purpose of this specific form of homeostatis is to keep blood flow constant when blood pressure varies which is done by expanding or contracting the layers of elastic tissue that compose the arteries. For example, when an increased amount of carbon dioxide is found in the blood, arteries will dilate to provide organs more oxygen and nutrients.

Two internal carotid arteries (ICAs) and two vertebral arteries (VAs) deliver oxygenated blood to the brain. See Figure 1.1 for a schematic. The blood then flows into the Circle of Willis (CoW). This circle of arteries near the center of the brain creates parallel paths of cerebral circulation. Thus if part of the CoW becomes occluded or is missing, other arteries can often preserve cerebral blood flow. It turns out, according to Lippert and Pabst (1985), that anatomical variations in the CoW are not uncommon; they affect up to 50% of humans (7). There is great variability in the arterial networks of humans which leads us to believe that a patient-specific approach must be used to study cerebral circulation. Thus, in this paper, patient-specific simulations are used for all the studies examined.

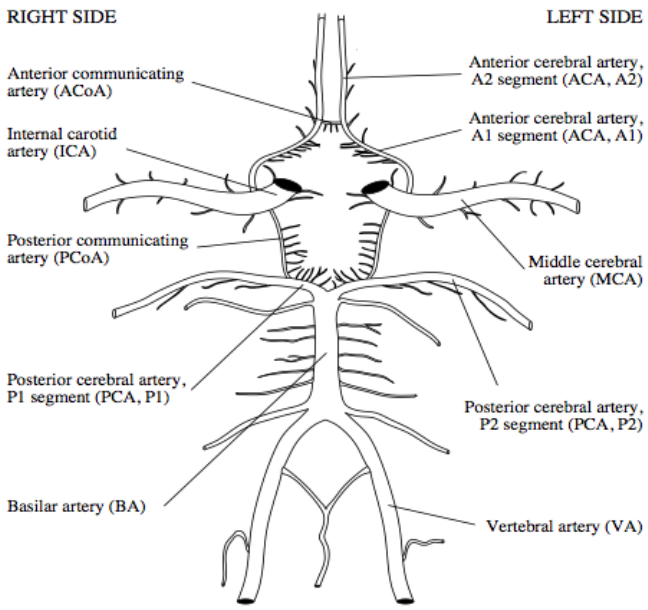

Figure 1.1: Circle of Willis - This figure is from (1)

Abnormalities in this arterial network can be the result of conditions such as stroke, vasospasm, vascular dementias, traumatic brain injury, and hydrocephalus. Too little blood in the cerebral arteries, ischemia, can lead to the death of brain tissue. Whereas too much blood, hyperemia, results in increased intercranial pressure, leading to a compression of brain tissue. Since abnormalities in cerebral circulation can lead to major complications or death, understanding the cerebral arterial network is of utmost importance. At the moment, most medical decisions concerning cerebral circulation do not account for the spatial and temporal scales present but instead solely rely on steady state conditions (e.g. mean cerebral blood flow).

Arterial blood flow in the human brain has been the subject of several mathematical studies. In one such study, Sherwin et. al (2003), a one-dimensional model (1D) of cerebral circulation was developed based on a non-linear, 1D algorithm which, using an elastic model of cerebral arteries, simulates blood flow wave propagation (8). This is the 1D model that this paper will focus on. The equations governing the 1D simulation are based on an impermeable and defomable tublar control volume of incompressible and Newtonian fluid (1). The equations modeling

flow in the 1D model come from the continuity and conservation of momentum equations from the discipline of fluid mechanics, respectively,

$$\frac{\partial A}{\partial t} + \frac{\partial (AU)}{\partial x} = 0$$

$$\frac{\partial U}{\partial t} + U\frac{\partial U}{\partial x} = -\frac{1}{\rho}\frac{\partial p}{\partial x} + \frac{f}{\rho A}$$

Here x is the axial position along a vessel, t represents time, ρ is the density of the blood, $A(x,t)$ is the cross-sectional area, $U(x,t)$ is the axial velocity averaged over the cross-section, and, similarly, $p(x,t)$ is the axial pressure averaged over the cross-section. The friction force per unit length, f, is equivalent to $-2\mu\pi\alpha/(\alpha-1)U$ where μ is the viscosity of the blood, taken as 4.5 mPa s, and α is a nondimensional correction factor dependent on the velocity profile.

To complete this system of differential equations, we use the pressure-area relationship, from (1),

$$p = \frac{\beta}{A_0}(\sqrt{A} - \sqrt{A_0}), \quad \beta = \beta_{scal}\frac{\sqrt{\pi}hE}{(1-\sigma^2)},$$

where A_0 is the reference cross-sectional area of the vessel, h is the reference arterial wall thickness, E represents Young's modulus, σ is Poisson's ratio, taken to be $\frac{1}{2}$, and β_{scal} is a scaling parameter of β. Thus β is a measure of the elasticity of the vessel. Descriptions of how bifurations and boundary conditions are handled can be found in (1).

2

Comparison of 1D and 3D Cerebral Circulation Simulations

2.1 Overview

Several different methods have been developed to study cerebral arterial flow. One method is the 1D simulation, mentioned above, which is described in (1; 8). Another simulation modeling the cerebral arterial network is a three-dimensional algorithm (3D). The 3D model is discussed in (3; 5).

Both methods, 1D and 3D, have benefits and limitations. The 1D simulation can both predict pulse wave propagation and model situations where blood flow does not exhibit strong 3D effects with reasonable accuracy. The model does well with small (diameter $<$ 2mm) arteries or, if applied to larger arteries, yields reasonable predictions of the large-scale features of the flow. Another benefit of the 1D simulation is that it is computationally inexpensive, taking less than an half an hour to run simulations of the CoW on a single processor. Yet this one dimensional model gives no data about local flow dynamics and can only model one direction of flow propagation, whereas blood flow is really multi-directional. For example, there is flow across the boundary of the vessel as plasma spreads into the surrounding tissue and there are also secondary flow patterns that arise in a curved vessel or at a bifurcation (2).

On the other hand, the 3D model allows us to more accuarately account for

the geometry of the blood vessels since it provides more information about flow patterns and Wall Sheer Stress. The 3D algorithm can accurately model the multiple directions of blood flow, such as the secondary flow that can occur by an artery bifurcation (2). Also, this algorithm can more accurately represent arteries since it accounts for the deformation of the arterial wall. Yet it takes significantly more time and computing power to run a simulation with the 3D algorithm. So if we are only interested in the mean flow, flow distribution, etc. the 1D simulation is a fast and efficient alternative.

Previous research has shown that both algorithms fairly accurately model arterial flow in the brain (1; 6). Therefore, we hope the results of the two methods will be complementary when used on the same arterial network. If so, the 1D model is a very powerful method since it is both fast and accurate.

Two different patients, both whom suffer from hydrocephalus and a CoW abnormality, were studied in this model comparison. The mission is not only to discern the potential of both models but also to gain a better understanding of cerebral flow. Perhaps the insights gained by studying brain abnormalities with algorithms of varying degree will give physicians a better understanding of the most effective treatments for such conditions.

The defining feature of hydrocephalus is an excessive accumulation of cerebrospinal fluid in the brain, which fills and widens the ventricles. The result is increased pressure in the brain since the brain cannot expand in response to the extra fluid. Thus there is increased pressure on brain tissue and arteries. This increased pressure leads to an extreme decrease in blood flow, which causes the brain to be starved of the nutrients it needs (4). This follows from Poiseuille's law, $F = \Delta P/R$ where F is the flow, ΔP is the internal pressure gradient, and R represents the resistance of the vessel. As intracranial pressure builds, it decreases the internal pressure gradient, yielding a decrease in flow. The most common treatment for hydrocephalus is to surgically insert a shunt which diverts the cerebrospinal fluid to another part of the body, most frequently the abdomen, where it can be absorbed. The flow of cerebrospinal fluid is then regulated by the shunt so as to maintain a constant intracranial pressure.

Simulations for a patients with a healthy brain and a complete or incomplete CoW are not discussed here but results for such simulations can be found in (1).

2.2 Methods

The 3D simulations were performed by Brown University PhD candidate, Leopold Grinberg. His 3D model used "patient-specific geometrical models of arterial networks, measured $in-vivo$ flowrates for the inlet boundary conditions, and the RC-type outflow boundary condition as a closure problem" with a "two-level domain decomposition and multi-level communicating interface" (5).

Two patient-specific arterial networks were obtained using MRI images from the Neurosurgery department of Children's Hospital in Boston (see Figure 2.1). In addition patient-specific flowrates, measured with PC-MRI at the ICAs and VAs, were obtained.

The two patient geometries we examined in this study are

(a) The right part of the CoW of Patient #1 who has hydrocephalus and an incomplete CoW

(b) An arterial network composed of the CoW and other arteries from Patient #2 who has hydrocephalus and an incomplete CoW

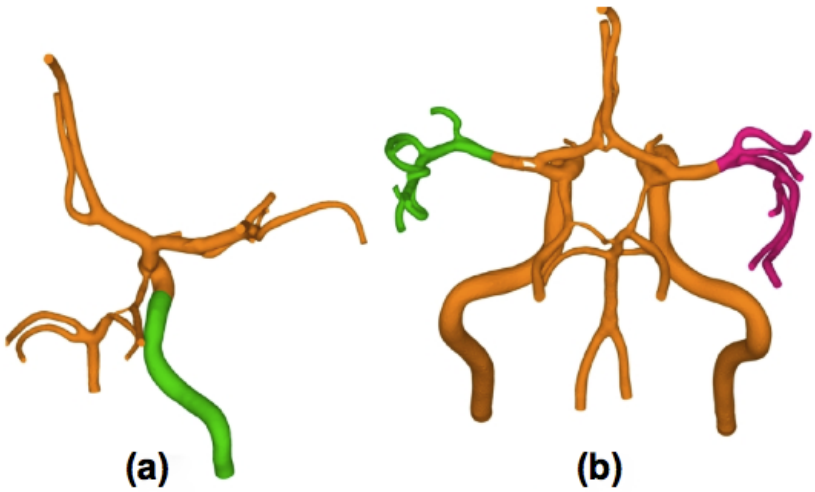

Figure 2.1: Cranial Geometries - (a) Right half of the CoW of Patient #1 who has hydrocephalus and an incomplete CoW; and (b) An arterial network composed of the CoW and other arteries from Patient #2 who has hydrocephalus and an incomplete CoW

Reconstruction of the arterial geometry was accomplished via gOREK software, developed at Brown University. The two patient geometries can be found in Figure 2.1. From the 3D reconstruction of the arteries, a 1D model of the arterial network was constructed using Tecplot. The 3D model was skeletonized (an example is shown in Figure 2.2) into a network composed solely of bifurcations. One limitation of the 1D model is that it only works on a network of bifurcations.

The arterial network was broken into segments, called domains, and arterial data was obtained for each domain. Using Tecplot, the length of each domain was measured using linear interpolation. The radius of each domain was calculated by taking slices of the artery, with Tecplot, and measuring the length from the arterial wall to the center of the artery. The radius was calculated three times per slice and slices were taken at three different points on each domain. The domain radius measurement used in the 1D simulation was the average of all radial measurements made on a domain.

Of course, there are some measurements which cannot be calculated with Tecplot. For each artery in our hydrocephalus arterial geometry, h and E were given the same values as a comparable artery in the Alastruey et al.'s patient geometry. The length of the cardiac cycle in this case is 1.1 seconds and we take $\rho = 1000\text{Kg*m}^{-3}$.

2.3 Patient #1

For the first comparison of the 1D and 3D models, a geometry only composed of the right half of the CoW for a patient with an incomplete CoW and hydrocephalus was chosen. Figure 2.2 shows the arterial network used for these simulations.

2.3.1 Methods

For this network, the 1D and 3D simulations used a rigid arterial wall model and the patient-specific flowrates at the two inlets were used as the input parameters. To make sure the 1D model was comparable to the 3D, in the 1D simulations the pressure at all terminal arteries was set to $p = 0$ and a sufficiently large β_{scal} value

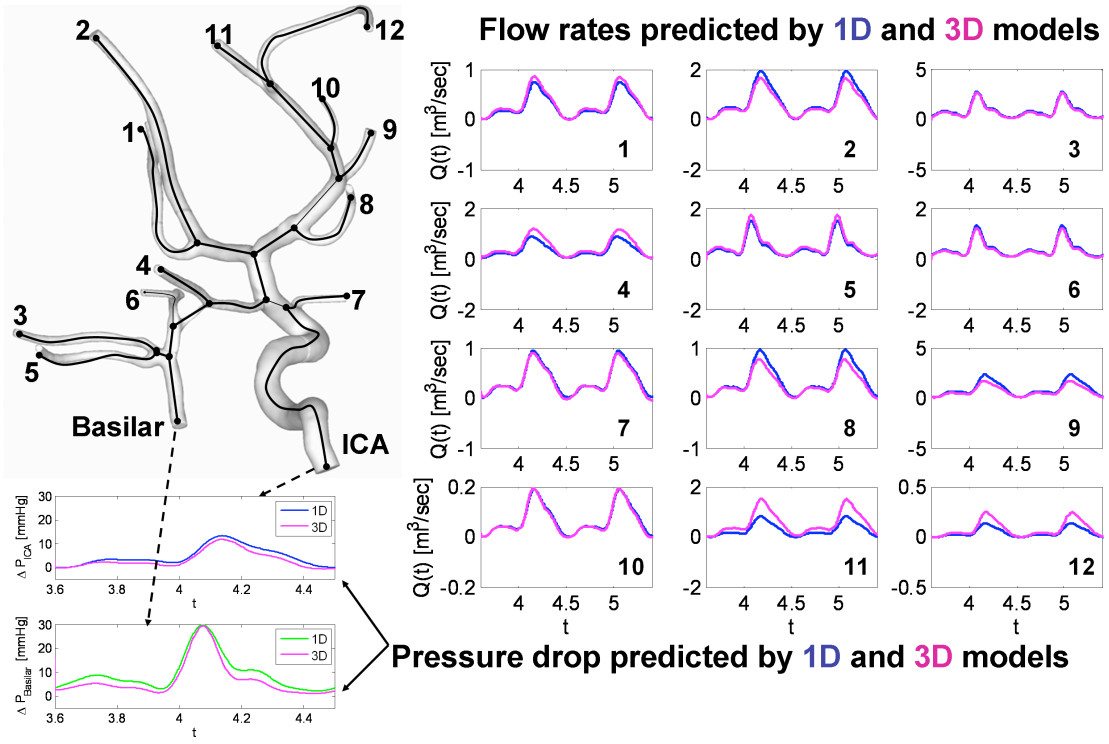

Figure 2.2: Simulation of Cerebral Circulation for Patient #1 Geometry - Blue represents 1D and magenta represents 3D. (Top left) Arterial geometry; (Bottom left) Pressure drop at (1) ICA, and (2) Basilar artery; (Right) Flow rates; 3D results provided by L. Grinberg (Brown University)

was used to stiffen the arterial walls. These two conditions imposed on the 1D model were meant to simplify the initial comparison of the 3D and 1D algorithms.

2.3.2 Results

Our model starts with all velocities at zero so each simulation was run for 8 cardiac cycles to make sure that the variability due to starting up circulation from zero velocity was eliminated. For our comparative analysis the last cardiac cycle is examined. Running the 3D model on this geometry took about 24 hours/cycle on 256 cores of CRAY XT4, whereas all 8 cycles in the 1D model took only 20 minutes on a single processor. Figure 2.2 shows the pressure drop between the terminal branches and the two inlets. Also the flowrates at each outlet are shown.

2.3.3 Discussion

Overall, we see remarkably consistent results for the 1D and 3D models. The disparities in the predicted flowrates are found in the vessels farthest from the inlet arteries (outlets 1,2 11, and 12). There are several reasons for the discrepancies in the predicted flowrates produced by the 1D and 3D models. One reason is that the 1D simulation does not model the angle of bifurcation for the arteries in the geometry. The 1D simulation models a bifurcation at a 90 degree angle and a bifurcation at 10 degree angle identically. Another shortcoming of the 1D model is that the velocity profile at all points in the arterial geometry is assumed to be the same. Therefore the affects of wall friction in arteries where swirling or reversal flow is found is not accurate. These are the primary reasons for the discrepancies. Though we should note again that the overall the flowrate predictions are extremely similar for the two models, even though the 1D model has limitations.

2.4 Patient #2

For this comparative analysis of the 1D and 3D models, a geometry composed of the major cranial arteries from a patient with an incomplete CoW and hydrocephalus, was used. Figure 2.3 shows the arterial network used for these simulations.

2.4.1 Methods

Instead of using a rigid arterial wall simulation for both the 1D and 3D models, as we did with Patient #1, for Patient #2 we allow the 1D simulation to model the elastic behavior of arterial walls. Two different values for β_{scal} ($\beta_{scal} = 1, 8$) were used to produce various levels of arterial elasticity. With these simulations we hope to uncover the difference in flowrate predictions and pressure drops among a rigid 3D model, a elastic 1D model ($\beta_{scal} = 1$), and a more rigid 1D model ($\beta_{scal} = 8$).

Using the method described in Section 2.2, the lengths and radii of the domains were measured and then the other parameters were estimated using data from Alastruey et. al. (2006). Table 2.1 summarizes this data for Patient #2.

There are four inlets in this patient geometry, the two internal carotid arteries (ICAs) and the two vertebral arteries (VAs). The same inlet boundary conditions,

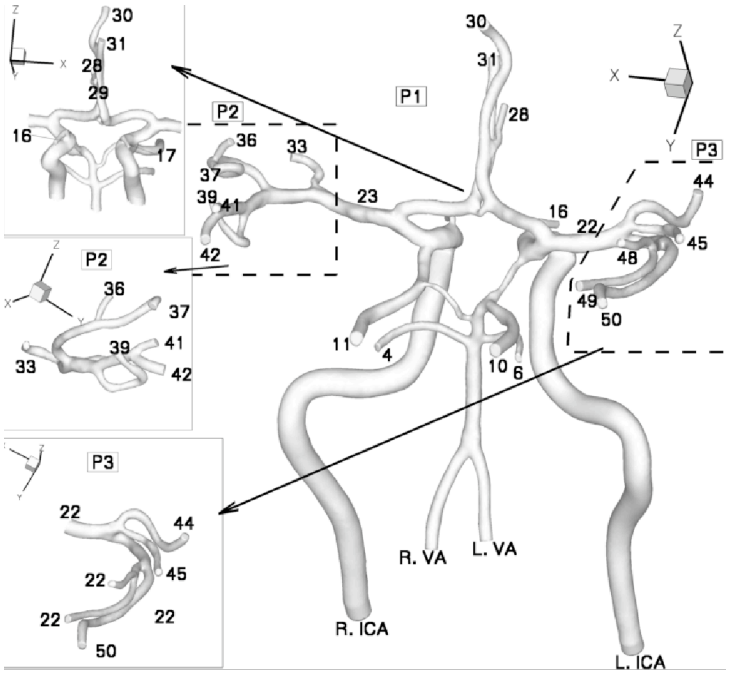

Figure 2.3: Arterial Network of Patient #2 - All outlets labeled with corresponding domain number. Geometry is broken into three parts - P1, P2, P3

patient-specific flowrates provided by Children's Hospital, were used for both the 1D and 3D models. These flowrates are shown in Figure 2.4. To convert this data to an input parameter, a Fourier series was used.

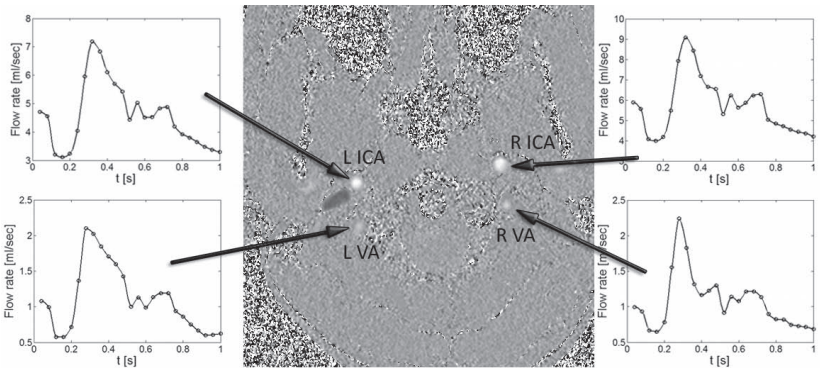

Figure 2.4: Patient specific flowrates at inlets - The inlet arteries in our geometry are the ICAs and the VAs. Flowrates at the four inlets were measured via PC-MRI.

The 3D model is composed of non-dimensional parameters but the 1D model

relies on dimensional variables. Thus conversion must be done to transform the parameters used in the 3D model into variables that can be used in the 1D simulation. To convert the non-dimensional pressure ($P_{non-dim}$), velocity ($U_{non-dim}$), flow rate ($Q_{non-dim}$), or resistance ($R_{non-dim}$) to dimensionalized pressure (P_{dim}), velocity (U_{dim}), flow rate (Q_{dim}), or resistance (R_{dim}), we multiply by a scaling parameter, $P^\star$, $U^\star$, $Q^\star$, or $R^\star$, respectively. This scaling factor contains the appropriate units so as to create a dimensionalized variable, for example, $Q_{dim} = Q_{non-dim} * Q^\star$. To calculate the scaling parameters, we have the following equations

$$\begin{aligned} P^\star &= \rho(U^\star)^2 \\ Q^\star &= U^\star * (L^\star)^2 \\ R^\star &= \frac{P^\star}{Q^\star} = \frac{\rho U^\star}{(L^\star)^2} \end{aligned}$$

$U^\star$ and $L^\star$ are obtained from the 3D model and ρ is taken as 1000Kg*m^{-3}.

To be able to compare 1D and 3D, both models used comparable boundary conditions for the terminal domains. The 3D algorithm uses a RC model for the distal end of each terminal artery but the 1D algorithm uses an RCR model. As found in Alastruey et al. (2006), the resistance parameter for the 1D model is called R_T and $R_T = R_1 + R_2$ where R_1 and R_2 are the two resistances used in the RCR boundary condition of the 3D model. R_1 is calculated as $\sqrt{\frac{\beta\rho}{2}}\left(A_0^{-\frac{3}{4}}\right)$ where $\rho = 1000$Kg*m^{-3} and β is equivalent to the parameter $\beta = \beta_{scal}\frac{\sqrt{\pi}hE}{(1-\sigma^2)}$ divided by A_0. R_2 is then calculated as $R_T - R_1$. When converting RC to RCR, we minimize R_1 and maximize R_2. To do this we set $R_T = R_{dim}$ since this results in R_1 becoming a tiny percentage (around 5%) of R_2. To calculate compliance C, we simply take $\frac{0.18}{R_{dim}}$. Resistance and compliance measurements for the 1D model can be found in Table 2.1.

2.4.2 Results

In Figures 2.5 and 2.6 you can see the results of the simulations. 3D data was provided by Leopold Grinberg (Brown University). For both algorithms, 7 cardiac cycles were run and data from the last cardiac cycle was analyzed.

2.4.3 Discussion

From Figure 2.5 it is easy to see that when $\beta_{scal} = 1$ there are noticeable differences in the amplitude for both flowrate and pressure drop along one cardiac cycle. But the average flowrate and pressure drop for both the 1D and 3D models match remarkably well. So when we run the 1D trial with $\beta_{scal} = 8$ we expect, since this causes a stiffening of arterial walls, that the amplitude of flowrate and pressure drop will converge to the corresponding 3D values. From Figure 2.5 we see that this is indeed the case; arrows on two of the graphs show that as β_{scal} increases, the 1D results converge to the 3D results. Therefore we must conclude that the difference in results is due to different modeling approaches, specifically a difference in the modeling of the elasticity of the arterial walls. While stiffening of the arteries can occur in humans, such as when a person ages, arterial walls are not always rigid. Thus it is of note that there is a discrepancy in the case of an elastic 1D model. In Figure 2.6, we show the cross-sectional area fluctuations at all the terminal arteries. For the case of $\beta_{scal} = 1$ we see fluctuations of less than 2%, which is physiologically acceptable. Typically an area fluctuation of such a small percentage would be ignored and a rigid arterial wall model would be taken to be accurate. But as we have seen from this simulation, small variations in area yield a significant contribution to the capacitance of a fairly large arterial geometry and have effects on all arteries in the system, even ones farthest from the inlets. Thus models of cerebral circulation should take into account the elasticity of arterial walls and more analysis of the affects of wall elasticity should be performed.

Domain	Length (m)	r (m)	h (m)	E (10^6 Pa)	R (10^9 Pa s m^{-3})	C (10^{-12} m^3Pa^{-1})
1 (R. VA)	0.1480	0.00136	0.00034	0.8	-	-
2 (L. VA)	0.1480	0.00136	0.00034	0.8	-	-
3 (Basilar)	0.0214	0.00104	0.00040	1.6	-	-
4	0.0860	0.00105	0.00026	1.6	36.8	4.89
5	0.001	0.00104	0.0004	1.6	-	-
6	0.086	0.00105	0.00026	1.6	36.8	4.89
7	0.0066	0.00104	0.0004	1.6	-	-
8	0.0045	0.00104	0.00027	1.6	-	-
9	0.0124	0.00052	0.00014	1.6	-	-
10	0.086	0.00105	0.00026	1.6	36.8	4.89
11	0.086	0.00105	0.00026	1.6	36.8	4.89
12	0.0151	0.00073	0.00018	1.6	-	-
13	0.0151	0.00073	0.00018	1.6	-	-
14 (L. ICA)	0.1703	0.00208	0.0005	0.8	-	-
15 (R. ICA)	0.1703	0.00223	0.0005	0.8	-	-
16	0.0071	0.00076	0.00026	1.6	73.6	2.45
17	0.0055	0.00056	0.00026	1.6	73.6	2.45
18	0.0067	0.00208	0.0005	0.8	-	-
19	0.0067	0.00223	0.0005	0.8	-	-
20	0.005	0.002	0.0005	1.6	-	-
21	0.005	0.002	0.0005	1.6	-	-
22	0.0144	0.00143	0.00036	1.6	36.8	4.89
23	0.0131	0.00143	0.00036	1.6	36.8	4.89
24	0.0117	0.00117	0.00029	1.6	-	-
25	0.0117	0.00117	0.00029	1.6	-	-
26	0.0114	0.00129	0.00026	1.6	-	-
27	0.0117	0.00142	0.00026	1.6	-	-
28	0.0093	0.00074	0.00019	1.6	36.8	4.89
29	0.0059	0.00084	0.00019	1.6	36.8	4.89
30	0.0249	0.00104	0.00026	1.6	36.8	4.89
31	0.0161	0.001	0.00026	1.6	36.8	4.89
32	0.0032	0.00074	0.00019	1.6	-	-
33	0.011	0.00074	0.00019	1.6	36.8	4.89
34	0.008	0.00137	0.00026	1.6	-	-
35	0.018	0.00085	0.00019	1.6	-	-
36	0.005	0.00072	0.00019	1.6	36.8	4.89
37	0.014	0.00088	0.00019	1.6	36.8	4.89
38	0.008	0.00137	0.00026	1.6	-	-
39	0.019	0.00066	0.00019	1.6	36.8	4.89
40	0.008	0.00106	0.00026	1.6	-	-
41	0.005	0.00073	0.00019	1.6	36.8	4.89
42	0.007	0.00103	0.00026	1.6	36.8	4.89
43	0.0022	0.0012	0.00026	1.6	-	-
44	0.0221	0.0011	0.00026	1.6	36.8	4.89
45	0.0171	0.0009	0.00019	1.6	36.8	4.89
46	0.0154	0.0012	0.00026	1.6	-	-
47	0.0092	0.0009	0.00019	1.6	-	-
48	0.0123	0.0014	0.00026	1.6	36.8	4.89
49	0.0243	0.0008	0.00019	1.6	36.8	4.89
50	0.0329	0.0011	0.00026	1.6	36.8	4.89

Table 2.1: Measurements for Patient #2 Geometry

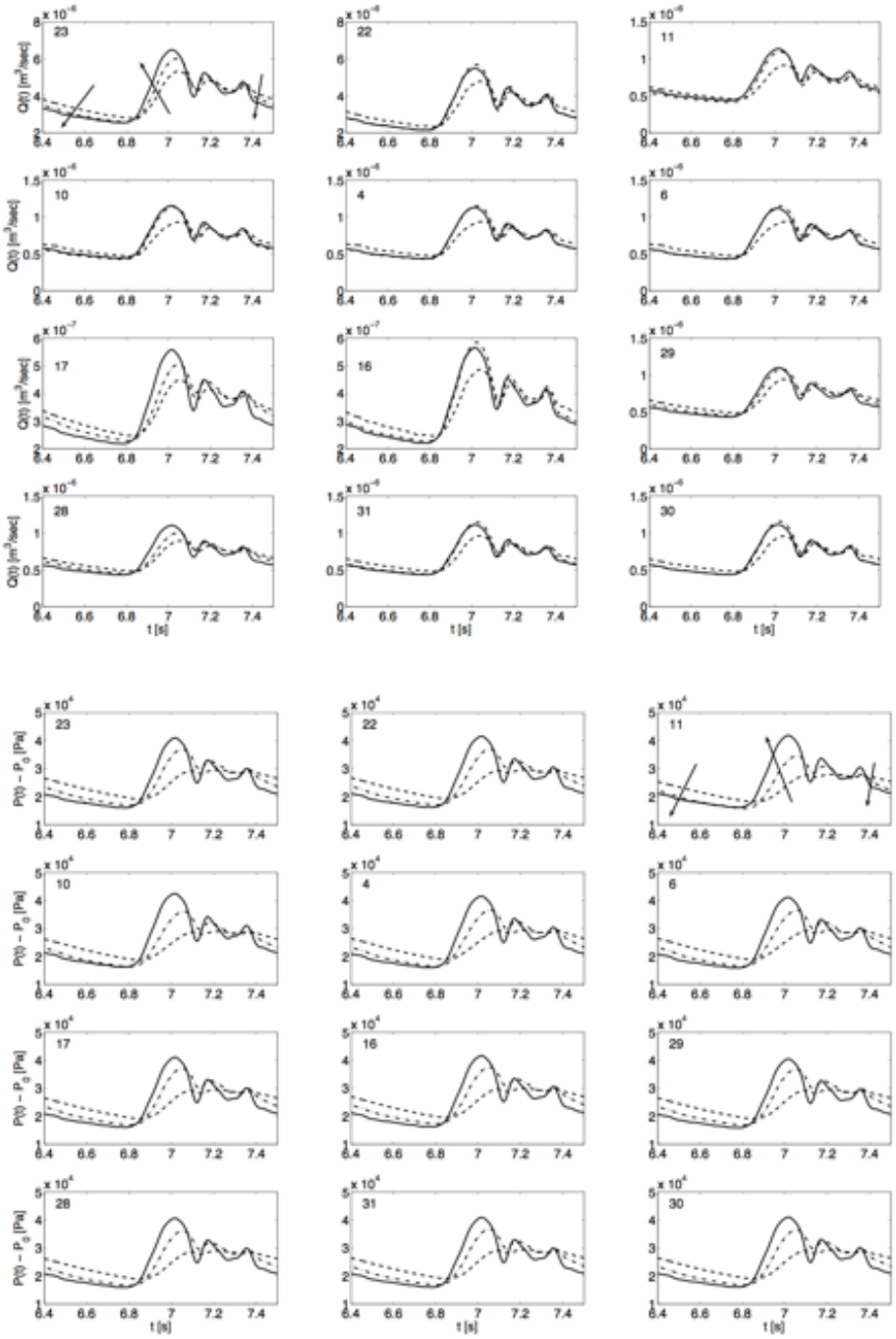

Figure 2.5: Comparison of flowrates and pressure-drops at P1 outlets - Simulation results for (bottom) pressure and (top) flowrate at outlets in P1 for Patient #2. Solid line – 3D model; Dashed line – 1D with elastic walls ($\beta_{scal} = 1$), and Dot-dashed line – 1D with stiff walls ($\beta_{scal} = 8$)

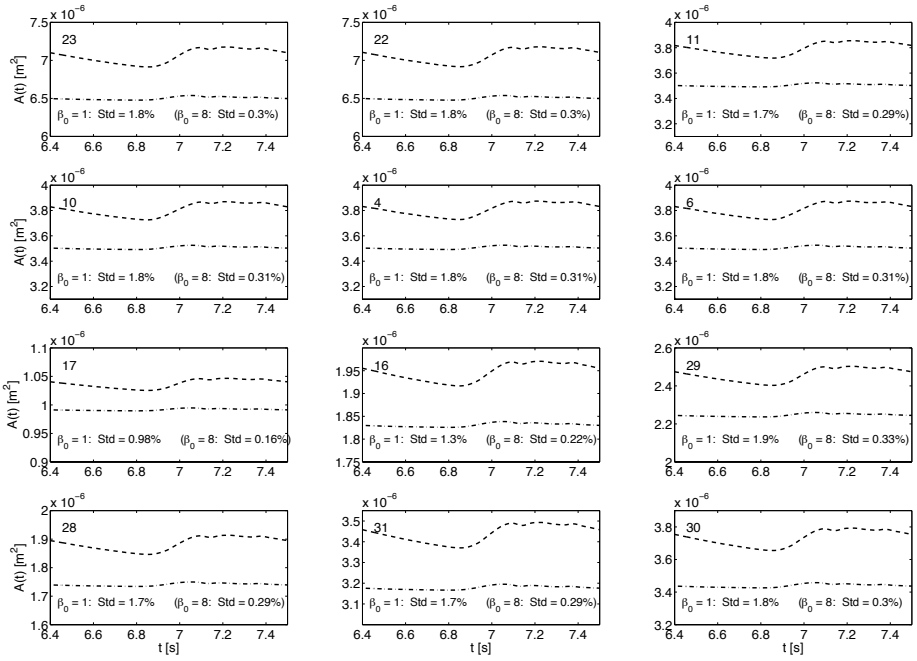

Figure 2.6: Comparison of cross-sectional area fluctuations at P1 outlets - Simulation results for flowrate at outlets in P1 for Patient #2. Dashed line – 1D with elastic walls ($\beta_{scal} = 1$), and Dot-dashed line – 1D with stiff walls ($\beta_{scal} = 8$); Standard deviation as a percentage of the mean is shown. β_0 is equivalent to the β_{scal} parameter

3

Sensitivity Study

3.1 Overview

The 1D model of cerebral blood flow is a computationally inexpensive and relatively accurate tool for understanding blood flow in the brain. But, as with any model, it is important to evaluate the robustness of this algorithm. We will do this through sensitivity analysis which is an approach to examining a model's response to changes in the input parameters. By understanding the relationship between the inputs and outputs of our simulation, we can better understand the structural formation of the model and better evaluate the validity of the model.

In this chapter, we will investigate the variation in pressure and flowrate when the elasticity of the arteries in the geometry is varied. As seen in the previous chapter, this is an important area of study. In our model, the parameter representing an artery's elasticity is β. Recall that

$$\beta = \beta_{scal} \frac{\sqrt{\pi} h E}{(1 - \sigma^2)}$$

where h the reference arterial wall thickness, E represents Young's modulus, and β_{scal} is a scaling parameter. The sensitivity study discussed here investigates the consequences of varying β from -25% to +25%, which is done through the use of β_{scal}. No other input parameters were changed during this study.

The input parameters for the 1D model, such as β, are already subject to several sources of error. As discussed in Chapter 2, lengths and radii of arteries for the 1D

model are measure in Tecplot which cannot yield completely accurate results. Also parameters which cannot be measured, such as wall thickness, are estimated. As a result, confidence in the output is already limited. But by studying the affects of substantial variation in β, we should be able to understand the degree to which inaccuracies in β influences the outputs of our model.

Two different arterial geometries are examined in this sensitivity studys

(a) Patient A: The arterial network of a healthy patient with a complete Circle of Willis. The CoW geometry is from (1) and an additional network of arteries was added to each middle cerebral artery (MCA). The geometry starts at the heart with the same cardiac input as in (1).

(b) Patient B: The geometry of a patient with hydrocephalus and an incomplete CoW. This is the geometry of Patient #1 from Chapter 2.

Pictures of these arterial networks can be found in Figure 3.1.

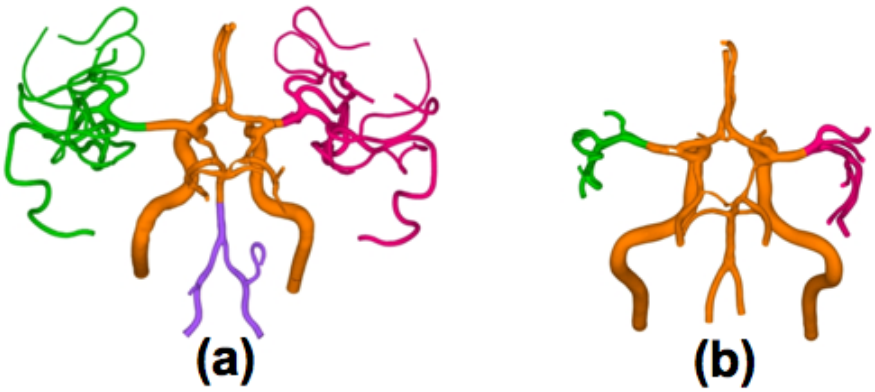

Figure 3.1: Cranial Geometries - (a) Geometry with full CoW and arterial networks off of the MCAs from Patient A who is healthy and has a full CoW – here all we show is the CoW and arteries off of the MCA even though simulation starts at the heart; (b) An arterial network composed of the CoW and other arteries from Patient B who has hydrocephalus and an incomplete CoW

3.2 Methods

A sampling-based, probabilistic sensitivity study is the method used here to evaluate the influence of fluctuations in artery elasticity. To preform such a study, simulations for varying, distinct values of β_{scal}, ranging from 0.75 to 1.25, were performed. Monte Carlo simulations, a process of using repeated random sampling to simulate a system, were used.

With this Monte Carlo sampling, our goal is to approximate the integral of $f(t, x, \beta_{scal})$ as the average of the function evaluated for many different β_{scal} values. $f(t, x, \beta_{scal})$ represents one of the outputs we are examining, flowrate or pressure, at time t, position x in the geometry, and with value β_{scal} used as the scaling parameter. Since we expect our system to be "well behaved", we can assume convergence if we do enough trials by the law of large numbers.

As a method of analyzing our results, the mean and standard deviation of $f(t, x, \beta_{scal})$ were computed. A position in the arterial network, x, was fixed and then the mean value of f for all time steps (t_k) was calculated by the formula

$$\bar{f}_{\beta_{scal}}(t_k) = \sum_{i=1}^{N} f(t_k, x, \beta_{scal_i}) * w_i$$

where N is the number of Monte Carlo trials performed. Each trial i, $1 \leq i \leq N$, is performed with a different value of β_{scal} and w_i is the weight corresponding to the value of β_{scal} for the trial. The standard deviation, σ_f, is calculated as

$$\sigma_{f_{\beta_{scal}}}(t_k) = \sqrt{\sum_{i=1}^{N} \left(\bar{f}_{\beta_{scal}}(t_k) - f(t_k, x, \beta_{scal_i})\right)^2 * w_i}$$

For the arterial geometry of Patient A we perform $N = 1000$ Monte Carlo simulations which is a sufficiently large enough N to obtain convergence. Since nothing is known about the probability distribution of β_{scal}, the uniform distribution is chosen as a valid guess. The β_{scal} parameters chosen for each trial were obtained by a random number generator drawing from the uniform distribution in the range of 0.75 to 1.25. From the choice of β_{scal} probability distribution it follows that each $w_i = 1/N$.

There is a cleverer way to perform the Monte Carlo simulations called Sparse Monte Carlo. This method was used on the geometry of Patient B, the patient with hydrocephalus. Sparse Monte Carlo is a more efficient method of numerical integration because it only samples the most important points which means faster convergence to the solution. These most important points, corresponding to the values taken on by the scaling parameter, were taken as Gauss-Legendre nodes. Legendre polynomials are used since this choice corresponds to drawing from the uniform distribution.

To select the appropriate number of nodes (N), three different simulations were performed ($N = 7, 9, 11$). Results did not reflect significant change from $N = 9$ to $N = 11$ so the results of the $N = 11$ trials will be analyzed in this chapter. Table 3.1 lists the nodes, in the 0.75 to 1.25 range, and corresponding weights used for the $N = 11$ simulation.

Trial	1	2	3	4	5	6	7	8	9	10	11
Nodes	1.2446	1.2218	1.1825	1.1298	1.0674	1.0	0.9326	0.8702	0.8175	0.7782	0.7554
Weights	0.0139	0.0314	0.0466	0.0583	0.0657	0.0682	0.0657	0.0583	0.0466	0.0314	0.0139

Table 3.1: Gauss-Legendre Nodes and Weights - Here $N = 11$ and nodes are taken from the range 0.75 to 1.25.

As mentioned above, only the value of β_{scal} changed in the various trials; all other input parameters stayed constant. Thus we can be confident that the changes in output values are due to the variations in artery elasticity.

To construct a 1D model of the Patient A geometry the arterial network, found in Figure 3.2 (middle), and corresponding parameter values were taken from (1). Then a patient's arterial network off of the MCA was obtained from Children's Hospital in Boston. This geometry was reconstructed from DSCTA and MRI images and then it was attached to both MCAs in the 1D geometry from (1). Figure 3.2 shows a schematic of how Patient A's geometry was constructed. The parameter values for the network which starts at the MCA were computed using the methods described in Section 2.2. Also found in Section 2.2 is a description of how the Patient B geometry was converted into a 1D network.

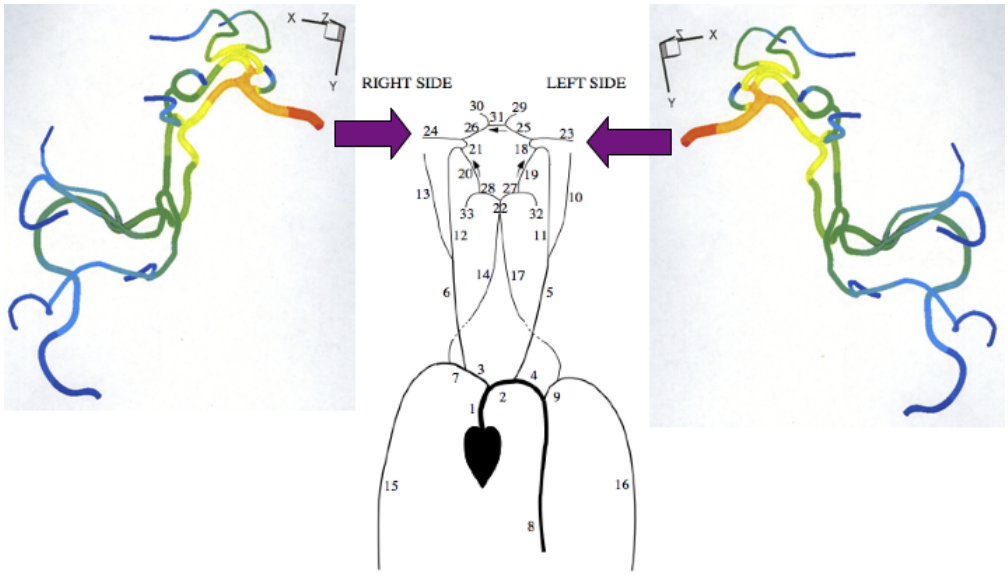

Figure 3.2: Construction of Patient A Geometry - In the middle is the 1D network used in (1). A network of arteries (left and right) were then added to the MCAs. This is depicted by the purple arrows. The network starting at the MCA is the same for the left and right side; the network off of the L. MCA is the mirror image of the network off of the R. MCA.

3.3 Results

3.3.1 Patient A

In this geometry, data was collected at 8 different locations in the arterial network. These locations are pictured in Figure 3.3. For domains 14, 23, 26, and 58 the data is taken at the midpoint of the artery whereas for domains 21, 33, 38, and 51 the data is taken as the terminal end of the artery.

At these 8 different locations, the mean pressure and flowrate are plotted over one cardiac cycle in Figures 3.7 and 3.8. In these figures, the shaded area represents the variation in pressure and flowrate, respectively, through the 1000 Monte Carlo trials. Tables 3.2 and 3.3 shows the minimum and maximum standard deviation in pressure and flowrate, respectively as a percentage of the mean.

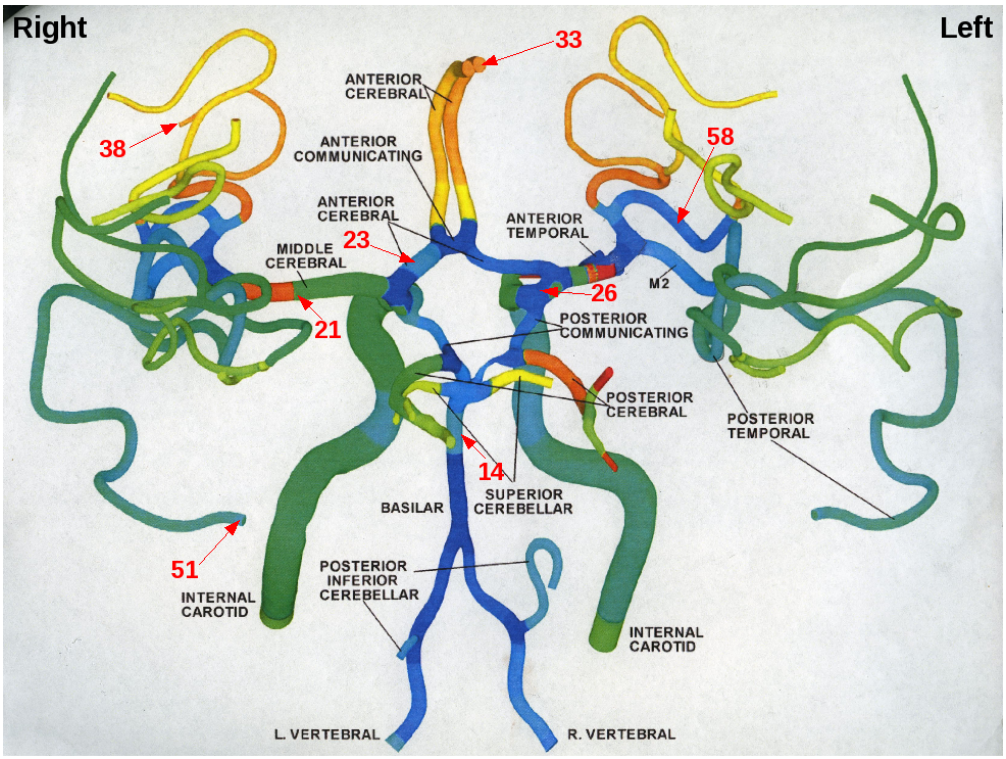

Figure 3.3: Locations where Output was Measured for Patient A - This is the arterial network for Patient A. The red arrows point to the 8 places where output was measured. The arrows are labeled with the corresponding domain numbers.

Domain	Min std	Max std
14	0.03072%	3.0729%
26	0.048103%	3.183%
23	0.22513%	3.7311%
21	0.081142%	3.6746%
33	0.16521%	3.2673%
56	0.12157%	3.4179%
58	0.1172%	3.6787%
51	0.15288%	4.0919%

Table 3.2: Minimum and Maximum Standard Deviation in Flowrate for Patient A - The minimum and maximum standard deviation in flowrate as a percentage of the mean for each point chosen in the geometry.

Domain	Min std	Max std
14	0.08088%	2.7389%
26	0.066094%	2.795%
23	0.045415%	2.8271%
21	0.029655%	2.2922%
33	0.10181%	2.8865%
56	0.029145%	2.3419%
58	0.038635%	2.3993%
51	0.034655%	2.3439%

Table 3.3: Minimum and Maximum Standard Deviation in Pressure for Patient A - The minimum and maximum standard deviation in pressure as a percentage of the mean for each point chosen in the geometry.

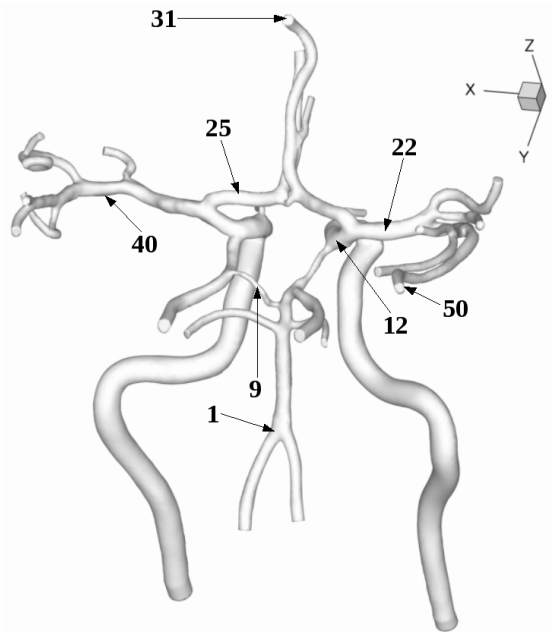

Figure 3.4: Locations where Output was Measured for Patient B - This is the arterial network for Patient B. The black arrows point to the 8 places where output was measured. The arrows are labeled with the corresponding domain numbers.

3.3.2 Patient B

In this geometry, data was collected at 8 different locations in the arterial network. These locations are pictured in Figure 3.4. For domains 9, 12, 22, 25, and 40 the

data is taken at the midpoint of the artery whereas for domains 1, 31, and 50 the data is taken as the terminal end of the artery.

At these 8 different locations, the mean pressure and flowrate are plotted over one cardiac cycle in Figures 3.9 and 3.10. In these figures, the shaded area represents the variation in pressure and flowrate, respectively, through the 11 Sparse Monte Carlo trials. Tables 3.4 and 3.5 shows the minimum and maximum standard deviation in pressure and flowrate, respectively as a percentage of the mean.

Domain	Min std	Max std
1	0.036823%	2.0623%
9	0.046142%	3.041%
12	0.18797%	3.0623%
22	0.034231%	1.6775%
25	0.046414%	2.9077%
31	0.031142%	1.9178%
40	0.046447%	1.5875%
50	0.020377%	2.0308%

Table 3.4: Standard Deviation in Flowrate for Patient B - The minimum and maximum standard deviation in flowrate as a percentage of the mean for each point chosen in the geometry.

Domain	Min std	Max std
1	0.060002%	1.6899%
9	0.055539%	1.5396%
12	0.053833%	1.5511%
22	0.052175%	1.4847%
25	0.051295%	1.5002%
31	0.049813%	1.4573%
40	0.047925%	1.4406%
50	0.051545%	1.4175%

Table 3.5: Standard Deviation in Pressure for Patient B - The minimum and maximum standard deviation in pressure as a percentage of the mean for each point chosen in the geometry.

3.4 Discussion

When looking at Figures 3.7, 3.8, 3.9, and 3.10 we see very similar results. For one, we see the most deviation in pressure when $\frac{\partial P}{\partial t}$ is small. We see the same behavior in flowrate. When there is a rapid acceleration in flowrate or pressure, there is hardly any deviation even multiple values of β_{scal} are being examined. Another commonality is that at these times of little standard deviation ($\frac{\partial P}{\partial t}$ is large), the pressure curve for a given value of β_{scal} switches which side of the mean it is on. The same behavior is seen with flowrate. Figures 3.5 and 3.6 show this occurrence in both flowrate and pressure for one specific value of β_{scal}. This flipping behavior is due to the fact that we are modeling a nonlinear system with a complex interconnected network of arteries.

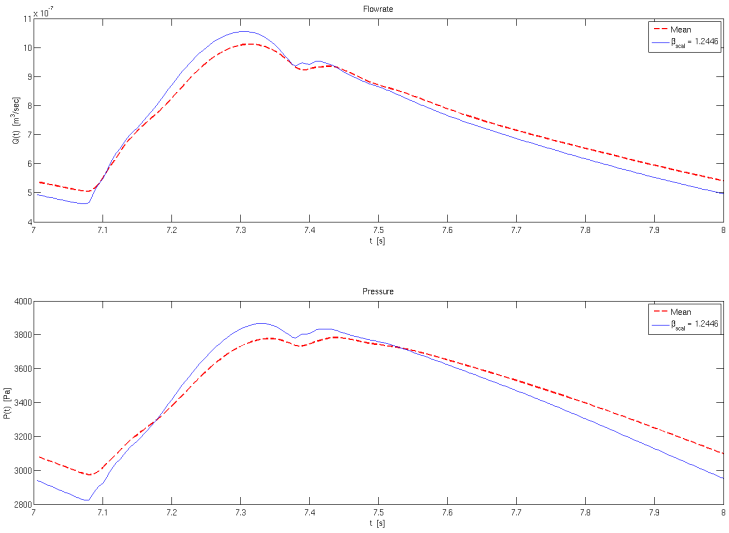

Figure 3.5: Alternating Behavior of Output with Regards to the Mean for Patient A - For $\beta_{scal} = 1.2446$, the output is shown in blue. Flowrate graph on top and pressure graph on bottom. Mean shown in red for both graphs.

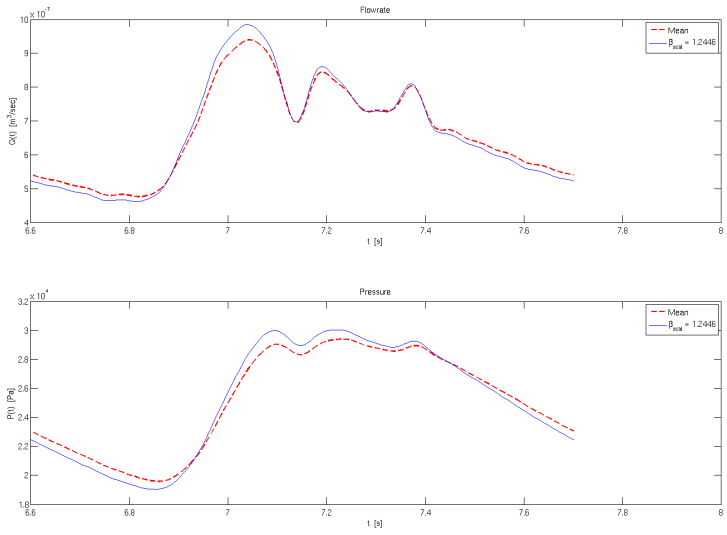

Figure 3.6: Alternating Behavior of Output with Regards to the Mean for Patient B - For $\beta_{scal} = 1.2446$, the output is shown in blue. Flowrate graph on top and pressure graph on bottom. Mean shown in red for both graphs.

Typically, in the Patient A geometry we see flowrate variations of less than or equal to 4% and pressure variations less than 3%. In Patient B we see the same behavior, except that the maximum variations are about one percentage less than in Patient A.

All variations are less than or equal to 4%. Variations of this order are so slight compared to the +/- 25% variation that the arteries of this network are undergoing. Therefore we conclude that the 1D model is robust to large variations in β. This result also tells us that our model will not be strongly affected by errors when calculating input β parameters. Having a robust model is key to aiding in the development of a 1D simulation that doctors can utilize to aid in diagnosis and treatment.

3.5 Graphs for Patient A and B

The order of the four figures in this section is as follows:

- Figure 3.7 - depicts the sensitivity of flowrate to changes in artery elasticity in the Patient A geometry
- Figure 3.8 - depicts the sensitivity of pressure to changes in artery elasticity in the Patient A geometry
- Figure 3.9 - depicts the sensitivity of flowrate to changes in artery elasticity in the Patient B geometry
- Figure 3.10 - depicts the sensitivity of pressure to changes in artery elasticity in the Patient B geometry

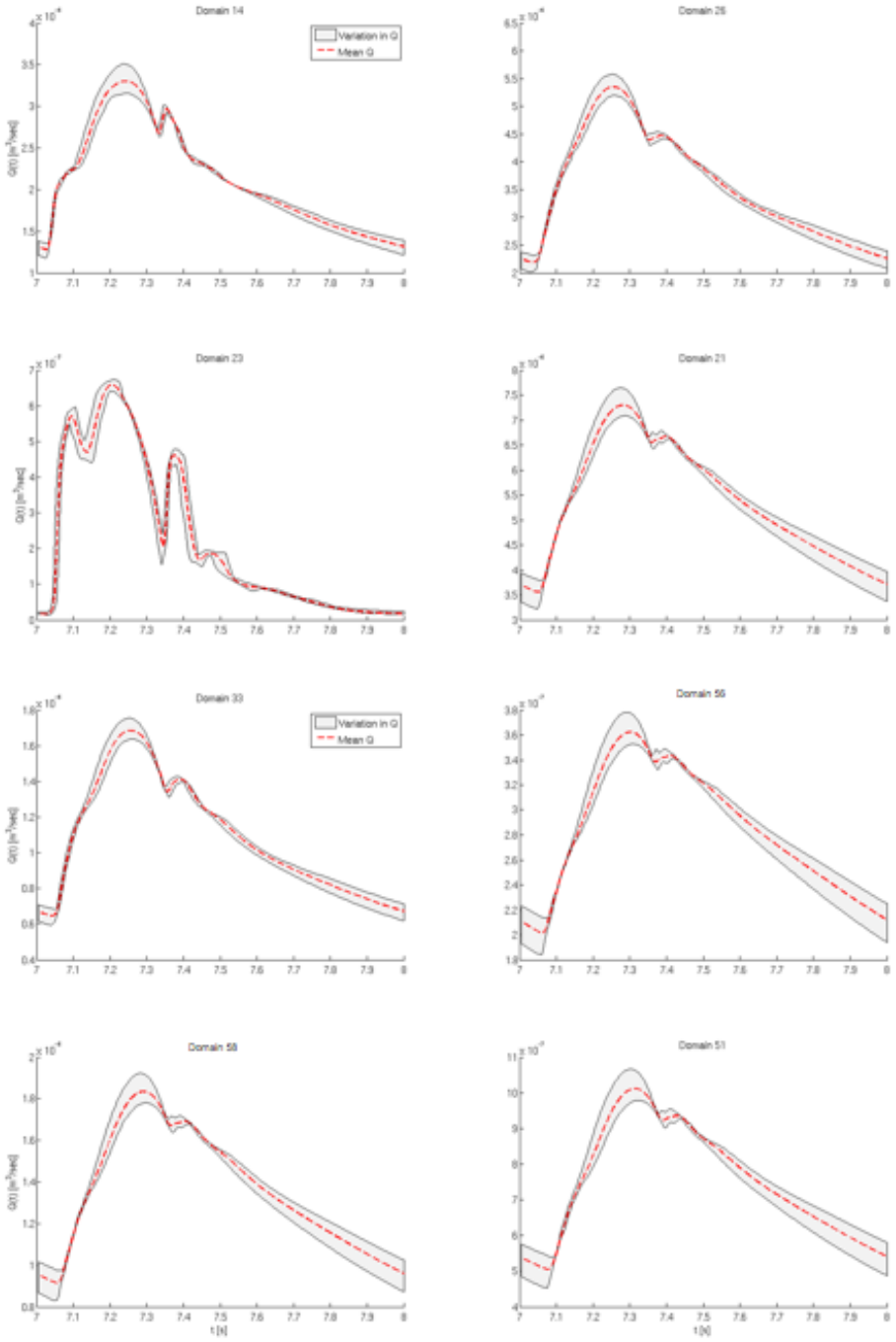

Figure 3.7: Sensitivity of Flowrate to Changes in Elasticity for Patient A - Shaded area represents the variations of flowrate. The red line shows the mean of the variations.

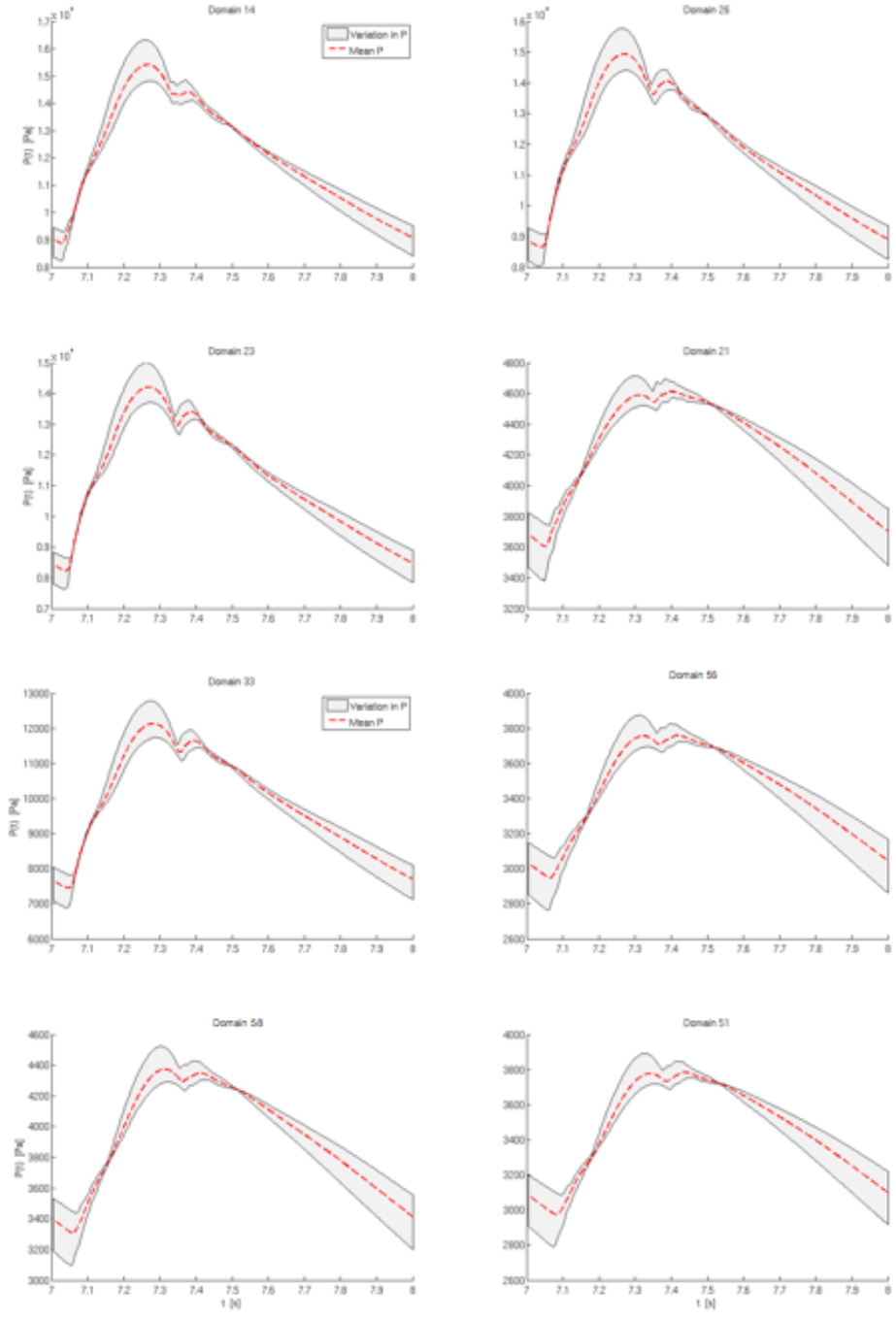

Figure 3.8: Sensitivity of Pressure to Changes in Elasticity for Patient A - Shaded area represents the variations of pressure. The red line shows the mean of the variations.

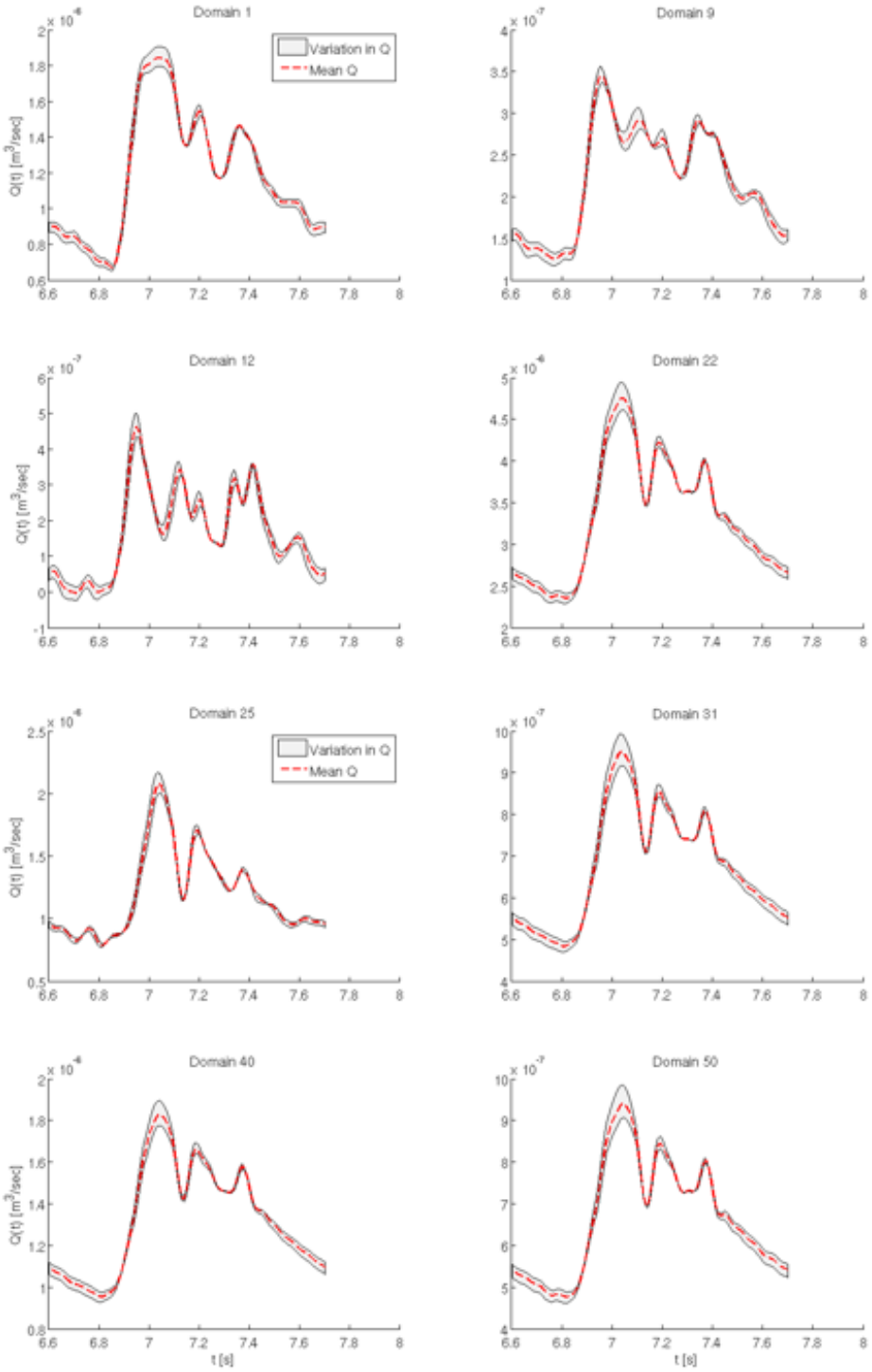

Figure 3.9: Sensitivity of Flowrate to Changes in Elasticity for Patient B - Shaded area represents the variations of flowrate. The red line shows the mean of the variations.

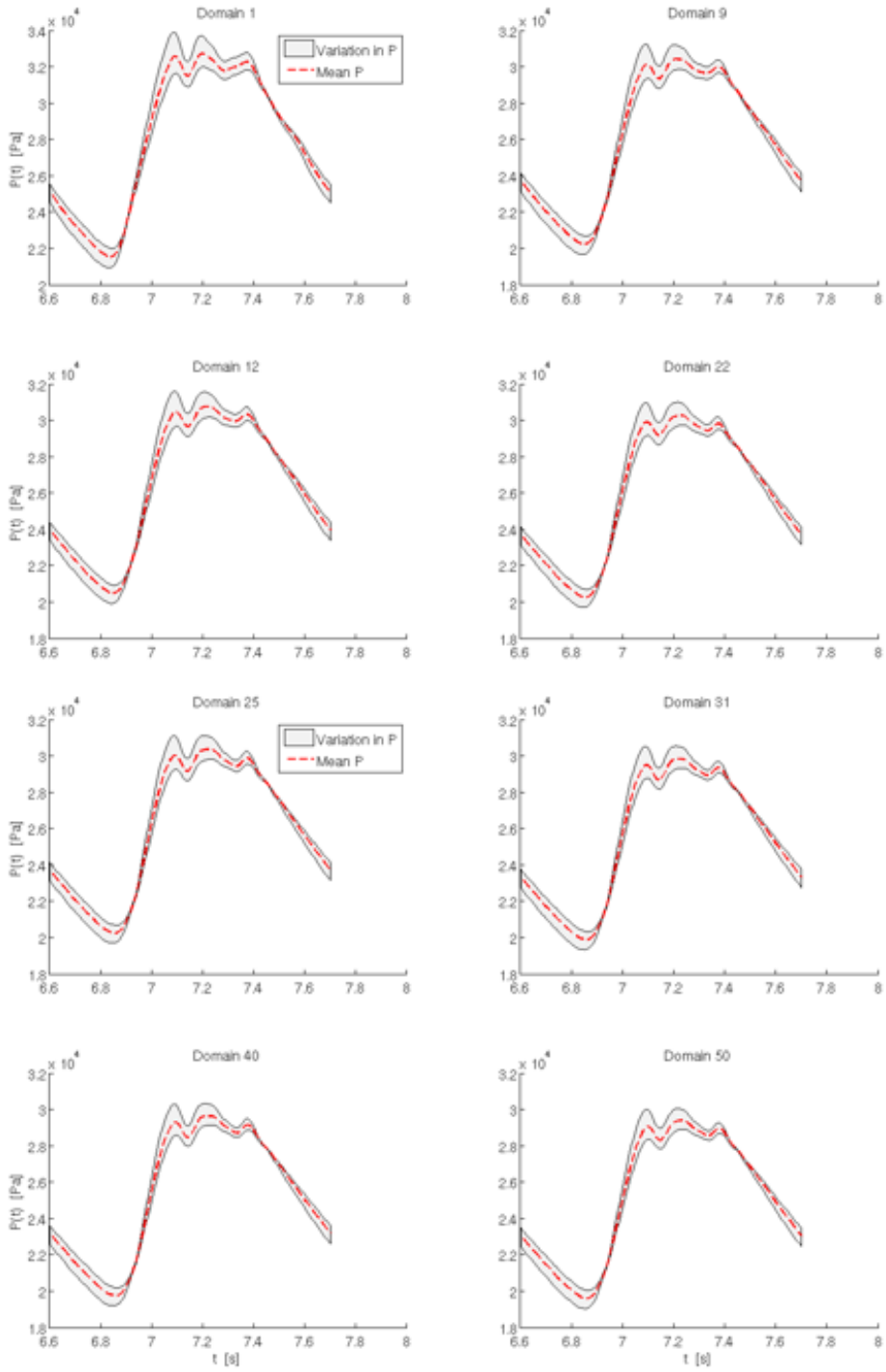

Figure 3.10: Sensitivity of Pressure to Changes in Elasticity for Patient B - Shaded area represents the variations of pressure. The red line shows the mean of the variations.

4

Conclusion

The human brain is a compelling area of study since this organ makes up 2% of body weight, receives 15% of the heart's output, and receives 20% of total body oxygen. Thus the brain is charged with the task of distributing a great percentage of cardiac output to surrounding tissue while staying bounded by the skull. The network of arteries that compose the blood flow pathways of the brain are extremely complex and also vary among all humans. Therefore a patient-specific approach of modeling cerebral blood flow must be taken.

A 1D and a 3D model of cerebral circulation have been developed and both simulate blood flow very accurately. While the 3D model can take into account more of the physiological parameters present in the arterial geometries, our studies show that the 1D model results match the 3D results well. Thus the 1D model is an accurate and fast alternative to the 3D algorithm.

In Chapter 2 we saw that it is important to take into account artery elasticity when modeling the cerebral arterial network. The importance of arterial elasticity on blood flow led us to examine the sensitivity of the 1D model to such variations. We see that even variations in elasticity by +/- 25% do not yield large variations in pressure or flowrate in the system. These results leave us confident that the model is robust when it comes to elasticity variations.

One hope of future work is to develop an arterial simulation that doctors can use in their offices. While the 3D model is an option for such a tool, its computational time makes it a poor choice for medical professionals who need results quickly in order to make diagnoses. Thus the 1D simulation is a better candidate

for doctors since it runs quite quickly and provides results comparable to the 3D model. Being able to use the 1D model in a doctor's office will require the development of a method to scan a patient's arterial tree, skeletonize it, and compute all needed input parameters for the 1D model. But, hopefully, one day such a tool will be available to medical professionals so that they can quickly find stenoses, aneurysms, and other arterial problems without an invasive procedure. Then they can understand the detrimental affects of these conditions on the patient's blood flow and determine the best course of treatment.

Bibliography

[1] J. Alastruey et al., *Modelling the circle of Willis to assess the effects of anatomical variations and occlusions on cerebral flows*, Journal of Biomechanics, 40: 1794-1805, 2006. 2, 3, 5, 6, 18, 20, 21

[2] Chen, Jie and Xi-Yun Lu, *Numerical investigation of the non-Newtonian blood flow in a bifurcation model with a non-planar branch*, Journal of Biomechanics, 37: 1899-1911, 2004. 5, 6

[3] S. Dong et al., *Simulating and visualizing the human arterial system on the TeraGrid*, Future Generation Computer Systems, 22.8: 1011-1017, 2006. 5

[4] Farrar Jr., J.K., and Margot R. Roach, *The Effects of Increased Intracranial Pressure on Flow Through Major Cerebral Arteries In Vitro*, Stroke, 4.5: 795-806, 1973. 6

[5] Grinberg, L., *Topics in Ultrascale Scientific Computing with Application in Biomedial Modeling*, PhD dissertation, Brown University, 2009. 5, 7

[6] Grinberg, L. and G. E. Karniadakis, *Outflow boundary conditions for arterial networks with multiple outlets*, Annals of Biomedical Engineering, 36: 1496-1514, 2008. 6

[7] Lippert, H. and R. Pabst, *Arterial Variations in Man: Classification and Frequency*, J.F. Bergmann, Munich. 1985. 1

[8] S. J. Sherwin et al., *One-dimensional modelling of a vascular network in space-time variables*, Journal of Engineering Mathematics, 47: 217-250, 2003. 2, 5